JVSTB Journal of Vacuum Science & Technology B

Mechanism of simultaneous formation of refractory-metal free C 40 and C 49 TiSi 2 induced by Q -switched Nd :Yttrium–aluminum–garnet laser irradiation

S. C. Tan, A. See, T. Yu, Z. X. Shen, and J. Lin

Citation: Journal of Vacuum Science & Technology B **23**, 480 (2005); doi: 10.1116/1.1868693
View online: http://dx.doi.org/10.1116/1.1868693
View Table of Contents: http://scitation.aip.org/content/avs/journal/jvstb/23/2?ver=pdfcov
Published by the AVS: Science & Technology of Materials, Interfaces, and Processing

Mechanism of simultaneous formation of refractory-metal free C40 and C49 $TiSi_2$ induced by *Q*-switched Nd:Yttrium–aluminum–garnet laser irradiation

S. C. Tan[a)]
Department of Physics, Blk S12, Faculty of Science, National University of Singapore, 2 Science Drive 3, Singapore 117542

A. See
Chartered Semiconductor Manufacturing Limited, 60 Woodlands Industrial Park D, Street 2, Singapore 738406

T. Yu, Z. X. Shen, and J. Lin
Department of Physics, Blk S12, Faculty of Science, National University of Singapore, 2 Science Drive 3, Singapore 117542

(Received 20 May 2004; accepted 10 January 2005; published 11 March 2005)

In this article, we demonstrate the usefulness of using a *Q*-switched Nd:Yttrium–aluminum–garnet laser to induce various phases of $TiSi_2$ in 350 Å of Ti layer deposited onto (100) Si substrates by varying the pulse width, τ, and energy fluence of the laser. Two sets of experiments were carried out. In the first set of experiments, τ and energy fluence of the laser are set at 0.18 μs and approximately 1.5 J/cm^2, respectively. The laser annealed Ti/Si sample was then characterized using micro-Raman spectroscopy and it was found that C49 $TiSi_2$ is formed at two different temperatures. One is formed at a nonmelting temperature, 680 °C, and the other formation temperature is at a high temperature of around 1975 °C. A mechanism is proposed to explain the formation of C49 under these two different conditions. In addition, we also note that C40 is formed between these two temperatures. In the second set of experiments, increasing τ to 1.6 μs and reducing the energy fluence to approximately 1.0 J/cm^2 resulted in the formation of pure refractory C40. This refractory metal free C40 phase is confirmed with glancing angle x-ray diffraction. © *2005 American Vacuum Society.* [DOI: 10.1116/1.1868693]

I. INTRODUCTION

Titanium disilicide ($TiSi_2$) has been successfully used in the semiconductor industry for ohmic contacts and gate electrodes in ultralarge-scale integrated circuits because it exhibits good chemical stability, self-passivation property in oxygen, and good selective formation when using the salicide process.[1] $TiSi_2$ may exist either as high resistivity C49 phase or as the low resistivity C54 phase.[2] In a typical Ti salicide process, there are two rapid thermal anneal (RTA) processes following Ti deposition. The first RTA at 620–680 °C forms the metastable C49 $TiSi_2$ phase. This high resistivity C49 $TiSi_2$ is transformed to the more stable C54 $TiSi_2$ at the second RTA at a temperature of around 850 °C. It has been widely reported that the kinetics of the C49–C54 phase transformation in $TiSi_2$ are adversely affected as the linewidth of the silicided region decreases.[3,4] This so-called "narrow line effect" occurs for thin $TiSi_2$ films because the C54 phase nucleates preferentially at C49 triple grain intersections.[5]

Because of this "narrow line effect" problem, the Ti salicide process cannot be extended to sub-0.25 μm technology and beyond. Several efforts have been made to achieve direct formation of C54 $TiSi_2$ bypassing the metastable C49 phase. Recently, Mouroux *et al.*,[6] Gribelyuk *et al.*[7] have achieved significant breakthroughs in the formation of C54 $TiSi_2$ through a C40 template. They have studied the formation of C54 $TiSi_2$ with a thin layer (~1 nm in thickness) of molybdenum deposited between Ti and Si substrate[6] or by implanting a small dose of Mo ions into Si substrate prior to Ti film deposition.[7] Upon annealing at 650 °C, a layer of C40 $(Ti,Mo)Si_2$ ternary phase was formed at the Ti and Si interface, which acts as a template, allowing the direct growth of C54 $TiSi_2$ on top. This method reduces the C54 $TiSi_2$ formation temperature by 100–150 °C as compared to the conventional method and at the same time bypasses the C49 phase.

From the process point of view, the deposition of a thin interposed layer (<2 nm) is difficult to reproduce. Moreover, additional refractory metal ion implantation causes integration issues. Therefore, new simple methods that could lead to the synthesis of refractory-metal-free C40 $TiSi_2$ are strongly desired. Our group[8] has recently reported that refractory-metal free C40 $TiSi_2$ on Ti/Si samples can be obtained by laser annealing. We identified the C40 $TiSi_2$ with micro-Raman and transmission electron microscopy (TEM). The crystal structure of this C40 $TiSi_2$ had been studied using high resolution TEM (HRTEM) by Li *et al.*[9] In this article, we report on the formation of C49 $TiSi_2$ at two different temperatures (i.e., 680 and 1975 °C, respectively) when blanket Ti/Si samples were annealed with a

[a)]Electronic mail: scip1187@hotmail.com

Nd:Yttrium–aluminum–garnet (YAG) laser with τ at 0.18 μs and with an energy fluence of approximately 1.5 J/cm^2. By increasing τ to 1.6 μs and reducing the energy fluence to approximately 1.0 J/cm^2 in another set of experiments, only pure C40 phase $TiSi_2$ was observed. The purpose of this article is to propose a mechanism for the anomalous formation temperature of C49 $TiSi_2$ and to report on the usefulness of using laser to induce $TiSi_2$ by varying the pulse width and energy fluence.

II. EXPERIMENT

Blanket Ti/Si samples were prepared from (100) oriented *p*-type *c*-Si substrates with a thin layer of Ti films (~350 Å) deposited on the substrate. Prior to the Ti deposition, the substrates were ultrasonically cleaned in SC1($NH_4OH:H_2O_2:H_2O=1:8:64$) and rinsed in hot de-ionized water. The substrates were then dipped into dilute HF to remove native oxide (SiO_2) followed by hot de-ionized water rinse. They were immediately loaded into a commercially rf sputtering chamber. Approximately 350 Å of Ti was then sputtered on the substrates.

Two sets of experiments (Sets 1 and 2) were conducted. In the first set of experiments, Ti/Si samples were irradiated with a *Q*-switched Nd:YAG laser ($\lambda=1.06$ μm, pulse width $\tau=0.18$ μs) with a repetition rate of 10 kHz and a laser fluence of ~1.4–1.6 J/cm^2. An atomic force microscope was used to study the topography of the irradiated sample after etching the sample in $NH_4OH:H_2O_2:H_2O=1:1:6$ to remove the unreacted metal. This sample was further studied using a Spex 1704 micro-Raman spectrometer with a 20 mW He–Ne laser ($\lambda=632.8$ nm) as the excitation source.

In the second experiment, the laser pulse width was increased to 1.6 μs and the laser fluence was set to approximately 0.9–1.1 J/cm^2 while keeping the repetition rate unchanged. All these laser annealing processes were done in air ambient. This sample was also characterized by the Spex 1704 micro-Raman spectrometer. A glancing angle x-ray diffraction (XRD) (GAXRD) was used to characterize the pure C40 $TiSi_2$. The XRD spectra were taken using a Bruker x-ray diffractometer. A Cu $K\alpha 1$ x-ray source was used at 40 kV and 40 mA. The incidence angle was set at 2° relative to the sample surface while the detector rotated to collect the diffracted x-ray. Atomic force microscopy (AFM) was also used to study the surface topography of the laser induced C40 $TiSi_2$ after etching in $NH_4OH:H_2O_2:H_2O=1:1:6$.

III. SIMULATION MODEL

For a better insight into the reaction mechanisms, it is critical to control the temperature during the process of the laser-materials interactions. Since it is quite difficult to obtain a direct measure of such parameters, a computer simulation is therefore carried out to determine the surface and interface temperatures.

In the computer simulation, the following assumptions are made:[10]

(1) the radiation density is uniform during the laser pulse time;
(2) the diameter of the laser beam interacting with the sample is much greater than the penetration depth of heat on the time scale of interest; and
(3) the composition of the sample is homogeneous in all directions except in the direction of penetration of the laser beam, where a metal–Si interface exists.

During the short pulse laser irradiation, the thermal diffusion distances are much smaller than the dimensions of the laser beam, limiting the gradients parallel to the surface to many orders of magnitude less than the gradients perpendicular to the surface.[11] Thus, we are able to simplify the problem adopting the one-dimensional heat flow equation with excellent approximation and accuracy.

The heat flow equation can be written as[10]

$$\rho_i(z,T)c_i(z,T)\frac{\partial T_i(z,t)}{\partial t}=\frac{\partial}{\partial z}\left[k_i(z,T)\frac{\partial T_i(z,t)}{\partial z}\right]+(1-R)I_0(t)\exp(-\alpha z),$$

where $i=$solid, molten phase; z and T are the direction of propagation of the beam and temperature respectively; $\rho(z,T)$, $c(z,T)$, and $k(z,T)$ are the density, the specific heat, and the thermal conductivity, respectively; R and α are the reflectivity and absorption coefficient of the material at the Nd:YAG laser wavelength; and $I_0(t)$ is the power density of incident laser. During laser annealing, the intense heat causes the surface to melt and the melt front rapidly moves down from the surface of the titanium film into the substrate. Such movement of the solid–liquid interface is strongly dependent on the thermal properties of the Si substrate. The difference in the melting point between the Ti film and the Si substrate may also lead to a discontinuous motion of the interface.[12]

The following boundary conditions are assumed:

(i) a perfect thermal contact at metal–Si interface, so that heat flux is continuous:

$$k_{\mathrm{Ti}}\frac{\partial T_{\mathrm{Ti}}}{\partial z}=k_{\mathrm{Si}}\frac{\partial T_{\mathrm{Si}}}{\partial z},$$

(ii) $T(z,0)=300$ K for all z;

$$\frac{\partial T}{\partial z}=0$$

when $z=0$, i.e., the heat loss by radiation or convection in a direction normal to the surface of the wafer is negligible.

(iii) $T(L,t)=300$ K, for all t, where L is the sample thickness; and
(iv) if a solid–liquid interface is present, the latent heat is released on melting at the interface.

Note that in above heat flow equation, $\rho(z,T)$, $c(z,T)$, $k(z,T)$ and $I(z,t)$ are all temperature and depth dependent, resulting in the unavailability of the analytical solutions in general cases. Therefore, computer-based numerical solutions are adopted. The heat flow equation was solved with

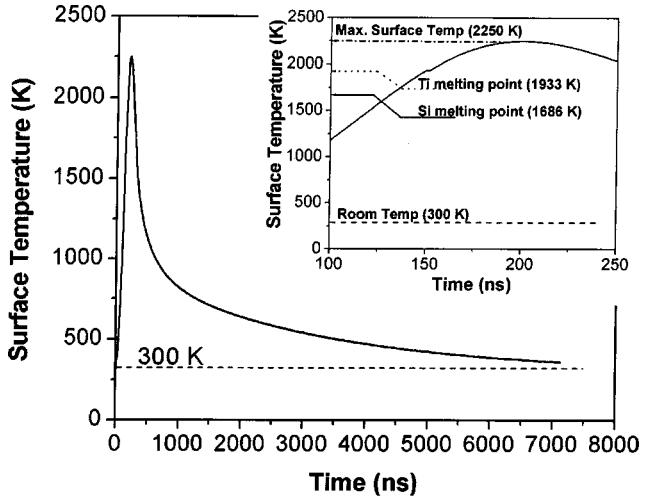

FIG. 1. Computer simulated temperature evolution on Ti surface after laser irradiation at an energy fluence of 1.6 J/cm^2.

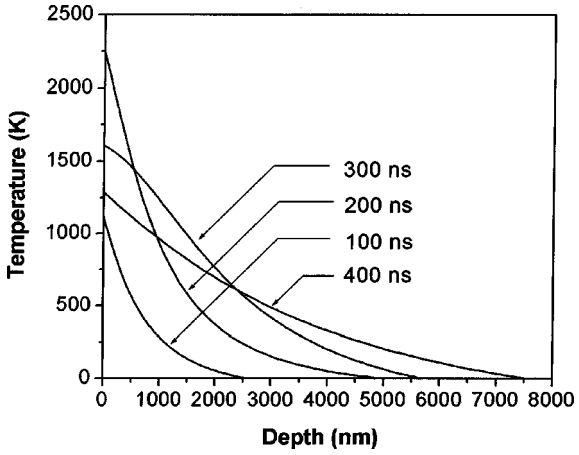

FIG. 2. Computer simulated temperature profile vs depth into the sample at different duration.

computer simulations using the finite difference method in our work with the appropriate sample and laser parameters.[13,14]

IV. RESULTS AND DISCUSSION

When the *Q*-switched Nd:YAG laser with a repetition rate of 10 kHz, pulse width τ of 0.18 μs, and laser fluence of approximately 1.4–1.6 J/cm^2 was incident on the set 1 samples, three distinct regions of A, B, and C (with a diameter of approximately 40 μm) were observed with a near Gaussian spatial distribution. After irradiation, the etched sample was first examined with an optical microscope. The Spex 1704 micro-Raman spectrometer was then used to study the phases formed at these three regions. Under the optical microscope, it was observed that the center region, which was irradiated with a higher intensity, has a very rough topography which was suspected to have melted. A computer simulation shows that the temperature at the surface rises from the ambient temperature to around 2250 K in 210 ns and cools down to room temperature within 9000 ns as indicated in Fig. 1. The ramping rate of the laser annealing process is therefore in the magnitude of 10^{10} K/s, while the cooling rate is also calculated to be on the order of 10^8 K/s. Figure 2 shows another series of simulations of the temperature distribution versus depth at different duration of $t=100$, 200, 300, and 400 ns. Note that the melting point of Ti and Si are 1933 and 1686 K, respectively. The temperature distribution versus depth graph at $t=200$ ns of Fig. 3 is the time before the temperature reaches its maximum value in our experiment. It is obvious that the temperature at the surface and Ti/Si interface are above the melting point of Ti and Si, indicating a melt consisting of Ti and Si atoms. A topographic AFM image of the laser irradiated region is shown in Fig. 4. The melted region at the center was labeled as region A and the region outside this melted region which experienced weaker laser intensity was labeled as region B and the near edges region was labeled as region C. Micro-Raman spectrometry (with a spatial resolution of $\sim$2 μm which is 20 times smaller than the laser spot size) was used to identify the phases present on the laser spot and it was found that the dominant phase in the melted region is C49 $TiSi_2$. This result is in good agreement with Shamma *et al.*[15] They have provided evidence of uniform melting as the primary cause of the formation of C49 $TiSi_2$ produced by laser annealing using an XeCl excimer laser at 308 nm. C49 $TiSi_2$ was formed in the center region, where it was exposed to the highest laser beam intensity, instead of the C54 phase because phase selection depends on the nucleation and growth kinetics of the competing product phases. As suggested by Boettinger and Perepezko,[16] a schematic representation of the role of nucleation and growth kinetics for phase selection as a function of processing conditions is represented by the metastable phase diagrams in Fig. 5. The thermodynamic relationships for the Gibbs free energy of the melt, the metastable C49 phase, and the stable C54 phase are shown in Fig. 5(a). Iannuzzi *et al.*[17] has used molecular-dynamics simulation to show that the melting point of C49 is about 250 K lower than that of the

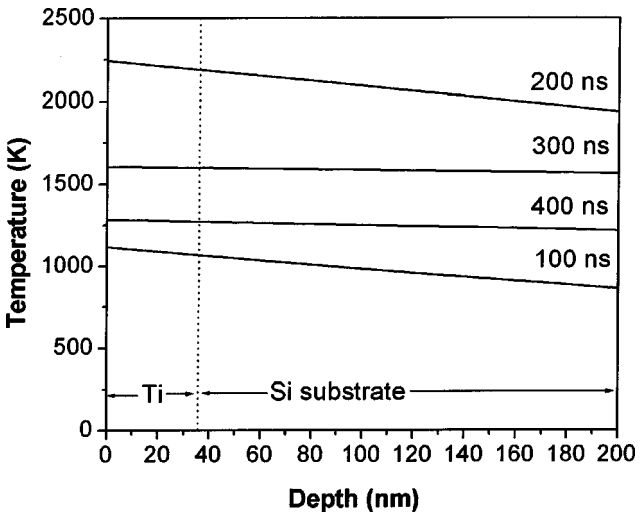

FIG. 3. Temperature profiles at the interface region.

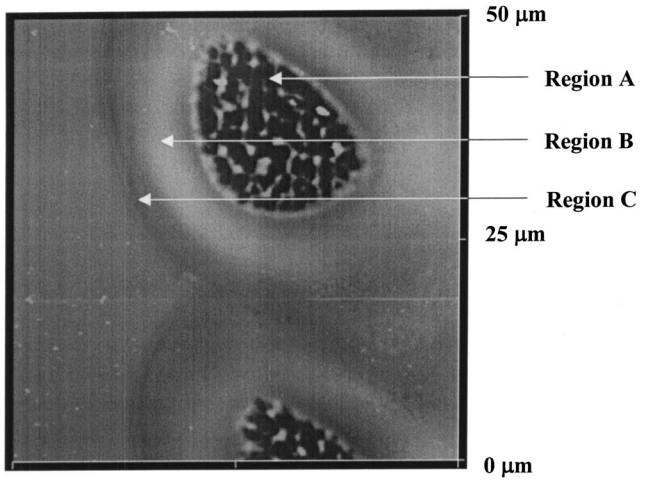

FIG. 4. AFM micrograph showing the topography of the irradiated Ti/Si sample.

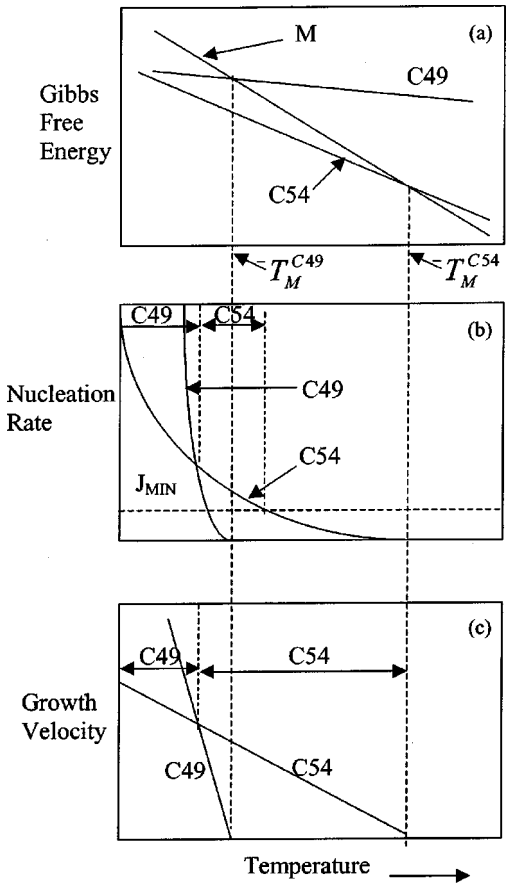

FIG. 5. Schematic representation of the operation of competitive phase selection kinetics which favors the formation of a metastable phase C49 $TiSi_2$ from the melt M at low temperature in spite of: (a) the thermodynamic stability of C54 $TiSi_2$. (b) Shows the temperature range for faster nucleation of C49 phase, while (c) shows the temperature range for faster growth of the C49 phase.

stable phase C54 $TiSi_2$. In addition, Boettinger and Perepezko[16] also suggest that a metastable phase will have a lower melting point than the stable phase. Hence the melting point of the metastable C49 and the stable C54 phase of $TiSi_2$ are indicated by T_M^{C49} and T_M^{C54} in Fig. 5(a), respectively. In the same figure, the intersections of the free energy curves correspond to the transition temperatures and the negative slope of either phase, $-dG/dT$ at constant pressure, is the entropy (S) of the phase. S is a measure of randomness or disorder of the system. For any substance, the solid state is more ordered than the liquid state, hence $S_{\text{solid}} < S_{\text{liquid}}$. Hence as shown in Fig. 5(a), the slope of the melt has the greatest gradient. We assume that C54 has a larger entropy than C49, this is because if C49 has a higher entropy than C54, the melting point of the C54 phase will be lower than that of the C49 phase. In Figs. 5(b) and 5(c), a possible pair of functions are depicted to illustrate the role of kinetics in phase selection under conditions that favor the nucleation and growth of the metastable phase.[16]

For the nucleation of C49 $TiSi_2$ or C54 $TiSi_2$ from the melt, the dominant product phase is determined to a large extent by the lowest value of the activation energy barrier for nucleation ΔG^* of C49 or C54 $TiSi_2$. The value of ΔG^* for each solid phase is a function of the amount of undercooling below the respective melting points and the liquid-crystal surface energy which acts as heterogeneous nucleation sites for C49 or C54 $TiSi_2$. As stated by Bergmann *et al.*,[18] a rapidly solidifying melt attempts to reduce its free energy as quickly as possible, rather than attaining its lowest possible free energy. This leads directly to a growth selection between metastable C49 $TiSi_2$ and stable phases C54 $TiSi_2$ and results in the formation of the metastable phase (i.e., C49 $TiSi_2$). In addition, Perepezko and Boettinger[19] also mentioned that during a rapid solidification process, the nucleation and/or the growth of a thermodynamically stable phase is difficult. Hence from the nucleation rate relationships presented in Fig. 5(b), we can see that the nucleation of C49 $TiSi_2$ dominates at lower temperatures. Figure 5(c) shows the growth rate of the C49 and C54 phases from the liquid as a function of interface temperature in a situation favoring metastable C49 $TiSi_2$ phase formation. With high cooling rate and large undercooling, the metastable C49 phase grows much faster than the stable C54 phase of $TiSi_2$. This explains why the C49 phase is the only phase present in the melt region. Iannuzzi *et al.*[17] simulations show that the melting point of C49 and C54 are 2800 and 3050 K, respectively. However in our simulations we show that the melt is cooled down from a temperature of 2250 K which means that if C49 phase nucleates faster than the C54 phase as shown in Fig. 5(a), then the melting point of C49 is definitely below 2250 K. On the other hand Archer *et al.*[20] predicted that the melting point of C54 is around 1700 K because in their experimental work they show that the differences in enthalpy increase significantly when C54 $TiSi_2$ was heated to a temperature of above 1500 K and they claim that such increases are usually observed in the temperature range prior to the melting point. If that is the case, our experimental results are closer with theirs.

Several micro-Raman spectra were taken at different positions in region B, which experienced lower laser beam in-

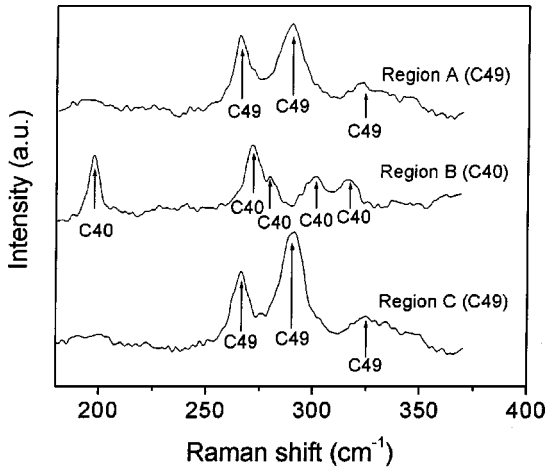

FIG. 6. General trend of the phases formed in these three regions with the use of a micro-Raman spectrometer.

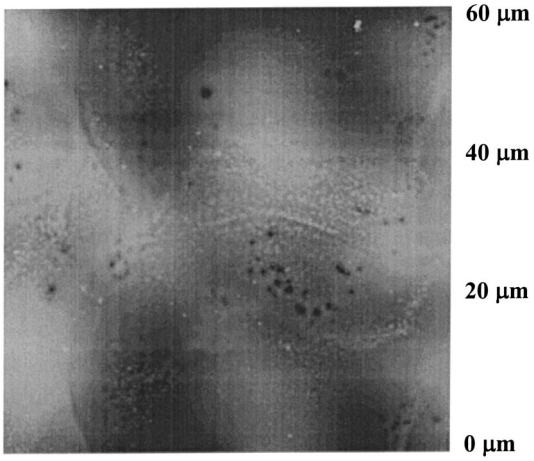

FIG. 7. AFM micrograph showing the topography of the C40 $TiSi_2$ after being exposed to the laser beam.

tensity. Most of the spectra taken in this region show the formation of C40 $TiSi_2$ and only a few spectra show the formation of C49 $TiSi_2$ at some random positions. A few spots were found to contain C49 $TiSi_2$ in this region because of some nonuniformity in the laser beam. On the other hand, most of the spectra taken from region C show C49 $TiSi_2$ and only a few spectra show the formation of C40 $TiSi_2$. Figure 6 shows the general trend of the phases formed in these three regions. As shown in Fig. 6 the dominant phase in region A is mainly C49 phase (268, 292, 326 cm^{-1}), the dominant phase in region B is mainly C40 phase (199, 272, 280, 301, 317 cm^{-1}), and lastly the dominant phase in region C is mainly C49 phase. This indicates that the formation temperature of laser induced C40 $TiSi_2$ is higher than C49 $TiSi_2$ when the reaction is solid state. C40 $TiSi_2$ was formed because of the extreme thermal nonequilibrium induced by laser annealing which leads to the predominance of the kinetic factors that favor its formation. C49 $TiSi_2$ can be formed at the melted region and the edges (i.e., not melted region) which show that there are two different mechanisms for the metastable C49 phase formation. The C49 phase that was formed in the region that is not melted was due mainly to diffusion, whereas the C49 phase that was formed in the melt region is believed to be due to the nucleation selection rules as stated in the previous paragraph. Further investigations into the effect of C49 $TiSi_2$ that forms from the melt on its transformation into C54 phase could be carried out.

When this laser pulse width was set to approximately 1.6 μs and the laser fluence was reduced to approximately 1.0 J/cm^2 while keeping the repetition rate the same, we were able to detect only C40 $TiSi_2$ from the Raman spectra (spectra not shown). C49 and C54 $TiSi_2$ are not observed in the Raman spectra after the laser irradiation. Figure 7 shows an AFM micrograph of two circular marks that were left on the Ti/Si sample after it had been exposed to the laser beam. Each circular mark is about 60 μm in diameter. The laser pulses are much bigger and uniform as compared to those in the first set of experiments. This shows that the temperature distribution of the laser beam incident on the sample was very uniform, which means that the thermal gradient in the formation of C40 in this set of experiments is very small as compared to the first set of experiments where the C40 phase was formed in region B where the thermal gradient was at its maximum. Hence we can conclude that it is possible to induce the formation of C40 phase under two different kinds of thermal gradients. It is more desirable to induce the formation of C40 using the second set of experiments because the thermal gradient is much smaller which also indicated that the thermal stress induced in the film is also at its minimum.

Approximately 400 000 of such circular pulses were created on a 1×1 cm^2 which was then characterized by GAXRD. The crystal structure of this refractory-metal free laser induced C40 $TiSi_2$ was first identified using HRTEM by Chen *et al.*[8] Recently Via *et al.*[21] have also shown that by depositing a thin layer of Ta at the Ti/Si interface, the C40 $TiSi_2$ was obtained after annealing at 525 °C from their Bragg–Bentano XRD results. In this article we discuss the observation of refractory-metal free laser induced C40 $TiSi_2$

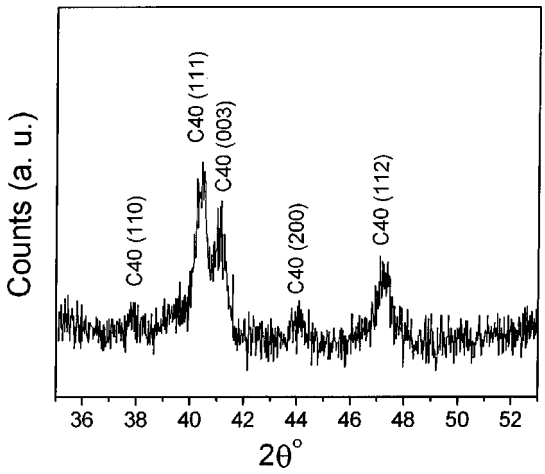

FIG. 8. GAXRD pattern of refractory-metal free C40 $TiSi_2$.

TABLE I. Experimental results of C40 $TiSi_2$ by different techniques.

Methods of forming C40 $TiSi_2$	Techniques used to find the lattice constants	a(Å)	c(Å)	References
Refractory-metal free C40 $TiSi_2$ (by laser annealing)	HRTEM	4.71	6.53	Li *et al.*[a]
By depositing a thin layer of Ta at the interface of Ti/Si followed by annealing at 525 °C	BBXRD	4.69	6.49	Via *et al.*[b]
Refractory-metal free C40 $TiSi_2$ (by laser annealing)	GAXRD (Present study)	4.67	6.59	Present study

[a]See Ref. 9.
[b]See Ref. 21.

by using a GAXRD. The GAXRD pattern in Fig. 8 shows five peaks at 37.98°, 40.43°, 41.05°, 43.93°, and 47.23°. Both the refractory-metal free and the refractory-metal doped C40 $TiSi_2$ obtained by Li *et al.*[9] and Via *et al.*,[21] respectively, have shown that the C40 $TiSi_2$ has a hexagonal structure with the space group $P6_222$. Therefore by assuming that the C40 $TiSi_2$ has a hexagonal structure, five peaks listed above are indexed as (110), (111), (003), (200), and (112), respectively. The experimental lattice constants calculated from the GAXRD pattern for this refractory-metal free laser induced C40 $TiSi_2$ are displayed in Table I. From Table I, the lattice constants of the refractory-metal free (by laser annealing) and the refractory-metal doped C40 $TiSi_2$, calculated by HRTEM, BBXRD, and GAXRD patterns, are in good agreement.

V. CONCLUSION

An interesting phenomenon was observed when the 350 Å Ti/Si sample was irradiated by a *Q*-switched Nd:YAG laser with a repetition rate of 10 kHz, a pulse width τ of 0.18 μs, and a fluence of approximately 1.4–1.6 J/cm^2. Under the optical microscope, it could be seen that the center region, which experienced the most intensity of the laser beam, shows signs of melting. This observation was further confirmed with our computer simulation results that the temperature at the center region is beyond the melting point of Ti and Si. However the region outside it showed no sign of melting. Raman spectra taken at the center region showed that only C49 $TiSi_2$ was present. Outside this center region, the dominant phase detected by micro-Raman spectra was C40 $TiSi_2$. However, Raman spectra taken at the outer edge of the laser pulse, showed mainly the C49 phase of $TiSi_2$. These results show that the formation of C49 phase can take place at two different temperatures: one is at a high temperature of around 1975 °C while the other is at 680 °C. In addition it also shows that the formation temperature of C40 $TiSi_2$ is inbetween these two temperatures. By increasing τ to 1.6 μs and reducing the energy fluence to approximately 1.0 J/cm^2 in another set of experiments, only the pure C40 phase $TiSi_2$ was observed. The lattice constants for C40 $TiSi_2$ are $a=4.67$ Å and $c=6.59$ Å, and were confirmed using GAXRD. Hence, we have shown that by varying the pulse width and energy fluence of the laser, we were able to produce uniform C40 $TiSi_2$ film. From the process point of view this technique is much faster as compared to other techniques[6,7] mentioned in Sec. I.

ACKNOWLEDGMENTS

The authors would like to thank Associate Professor Andrew Wee Thye Shen and Dr. William J. Boettinger for the valuable discussion.

[1]S. R. Muraka, *Silicides for VLSI Applications* (Academic, New York, 1983).
[2]R. Beyers and R. Sinclair, J. Appl. Phys. **57**, 5240 (1985).
[3]J. B. Lasky, J. S. Nakos, O. J. Cain, and P. J. Geiss, IEEE Trans. Electron Devices **38**, 262 (1991).
[4]S. Privitera, F. La Via, M. G. Grimaldi, and E. Rimini, Appl. Phys. Lett. **73**, 3863 (1998).
[5]Z. Ma, L. H. Allen, and D. D. J. Allman, Thin Solid Films **253**, 451 (1994).
[6]A. Mouroux, S.-L. Zhang, W. Kaplan, S. Nygren, M. Östling, and C. S. Petersson, Appl. Phys. Lett. **69**, 975 (1996).
[7]M. A. Gribelyuk, J. A. Kittl, and S. B. Samavedam, Appl. Phys. Lett. **86**, 2571 (1999).
[8]S. Y. Chen, Z. X. Shen, K. Li, A. K. See, and L. H. Chan, Appl. Phys. Lett. **77**, 4395 (2000).
[9]K. Li, S. Y. Chen, and Z. X. Shen, Appl. Phys. Lett. **78**, 3989 (2001).
[10]M. Bertoloti, *Physical Process in Laser-Materials Interactions* (Plenum, New York).
[11]R. K. Singh and J. Viatella, JOM **44**, 20 (1992).
[12]R. K. Singh, K. Jagannadham, and J. Narayan, J. Mater. Res. **3**, 1119 (1988).
[13]Y. S. Touloukian, *Thermal Properties of High Temperature Solid Materials* (Macmillian, New York, 1969), Vol. 4.
[14]G. Gorachand, *Handbook of Thermo-Optic Coefficients of Optical Materials with Applications* (Academic, New York, 1998).
[15]N. Shamma, S. Talwar, G. Verma, K. J. Kramer, N. Farrar, C. Chi, W. Greene, and K. Weiner, Mater. Res. Soc. Symp. Proc. **470**, 265 (1997).
[16]W. J. Boettinger and J. H. Perepezko, in *Rapidly Solidified Alloys*, edited by H. H. Libermann (Marcel Dekker, Inc., New York, 1993).
[17]M. Iannuzzi, L. Migilio, and M. Celino, Phys. Rev. B **61**, 14405 (2000).
[18]H. W. Bergmann, G. Barton, B. L. Mordike, and H. U. Fritsch, Mater. Res. Soc. Symp. Proc. **28**, 29 (1984).
[19]J. H. Perepezko and W. J. Boettinger, Mater. Res. Soc. Symp. Proc. **19**, 223 (1983).
[20]D. G. Archer, M. S. Sabella, S. E. Stillman, and E. J. Cotts, J. Chem. Eng. Data **40**, 1237 (1995).
[21]F. La Via, F. Mammolitti, G. Corallo, M. G. Grimaldi, D. B. Migas, and L. Miglio, Appl. Phys. Lett. **78**, 1864 (2001).